Supplementary Material for: "Making Trotters Sprint: A Variational Imaginary Time Ansatz for Quantum Many-Body Systems"

Matthew J. S. Beach,[1,2] Roger G. Melko,[1,2] Tarun Grover,[3] and Timothy H. Hsieh[1]

[1] *Perimeter Institute for Theoretical Physics, Waterloo, Ontario N2L 2Y5, Canada*
[2] *Department of Physics and Astronomy, University of Waterloo, Waterloo N2L 3G1, Canada*
[3] *Department of Physics, University of California at San Diego, La Jolla, CA 92093, USA*

(Dated: August 19, 2019)

JORDAN-WIGNER TRANSFORMATION

The 1d TFIM conveniently admits a solution via the Jordan-Wigner transformation [1], where L Ising spins are mapped to $L/2$ independent spin-$\frac{1}{2}$ fermions by introducing the fermionic operators

$$a_j = e^{i\pi\phi_j} S_j^-, \qquad a_j^\dagger = e^{-i\pi\phi_j} S_j^+, \tag{1}$$

with $\phi_j = \sum_{i=1}^{j-1} S_i^+ S_i^-$ and where $S_j^\pm = (Y_j \pm iZ_j)/2$ are the raising/lowering operators. Performing a Fourier transform, we have

$$\begin{aligned} H_{ZZ} &= \sum_{k=0}^{L-1} \left(2c_k^\dagger c_k - 1\right) \\ H_X &= 2 \sum_{k=0}^{(L-1)/2} \cos\theta_k \left(c_k^\dagger c_k + c_{-k}^\dagger c_{-k}\right) \\ &\quad + i \sin\theta_k \left(c_k^\dagger c_k + c_{-k}^\dagger c_{-k}\right) \end{aligned}$$

with $\theta_k = \frac{(2k+1)\pi}{L}$. We abbreviate the terms in the sums as $H_{ZZ}(k)$ and $H_X(k)$ respectively. The VITA then amounts to the decoupled expression

$$|\psi_P(\boldsymbol{\alpha},\boldsymbol{\beta})\rangle = \bigotimes_{k=0}^{(L-1)/2} \prod_{p=P}^{1} e^{-\beta_p H_X(k)} e^{-\alpha_p H_{ZZ}(k)} |0_k 0_{-k}\rangle \ .$$

Since the true ground state of the TFIM Hamiltonian is known, we can compute the fidelity directly. The exact ground state is given by

$$|\psi_{\text{exact}}\rangle = \bigotimes_{k=1}^{N/2} \left(u_k + v_k c_k^\dagger c_{-k}^\dagger\right) |0_k 0_{-k}\rangle \ . \tag{2}$$

with

$$\begin{aligned} u_k &= \sqrt{\frac{E_k + \zeta_k}{2E_k}}, \qquad v_k = i\sqrt{\frac{E_k - \zeta_k}{2E_k}}, \\ E_k &= \sqrt{J^2 + h^2 + 2Jh\cos\theta_k}, \\ \zeta_k &= -h - J\cos\theta_k \ . \end{aligned}$$

Entanglement Entropy

Because the TFIM is dual to a free system, all correlations, and hence the entanglement entropy (EE), can be determined from the two-point functions by Wick's theorem [2, 3]. It is convenient to introduce Marjorana fermions $a_{2n} = i(c_n - c_n^\dagger)$, $a_{2n-1} = c_n + c_n^\dagger$ with the $2L \times 2L$ correlation matrix $\langle a_n a_m\rangle = M_{nm} = \delta_{nm} + i\Gamma_{nm}$ given by

$$\Gamma_{ij} = \begin{pmatrix} \Pi_0 & \Pi_1 & \cdots & \Pi_{L-1} \\ \Pi_{-1} & \Pi_0 & & \vdots \\ \vdots & & \ddots & \vdots \\ \Pi_{1-L} & \cdots & \cdots & \Pi_0 \end{pmatrix}, \qquad \Pi_n = \begin{pmatrix} 0 & g_n \\ -g_{-n} & 0 \end{pmatrix} \tag{3}$$

with

$$g_n = \langle a_n a_0\rangle = \langle c_n^\dagger c_0^\dagger\rangle + \langle c_n^\dagger c_0\rangle - \langle c_n c_0\rangle - \langle c_n c_0^\dagger\rangle \tag{4}$$

The correlation functions can be found from their Fourier transforms,

$$\langle c_k c_{-k}\rangle = u_k v_k^* \tag{5}$$
$$\langle c_k^\dagger c_{-k}^\dagger\rangle = u_k v_k^* \tag{6}$$
$$\langle c_k^\dagger c_k\rangle = v_k^2 \tag{7}$$
$$\langle c_k c_k^\dagger\rangle = u_k^2 \tag{8}$$

Using these expressions to compute g_n, we have

$$g_n = \frac{2}{L} \sum_{k=0}^{(L-1)/2} \left(2\tilde{u}_k \tilde{v}_k \sin n\theta_k + \left(\tilde{u}_k^2 - \tilde{v}_k^2\right)\cos n\theta_k\right) \tag{9}$$

where $\tilde{u}_k, \tilde{v}_k$ are real numbers that characterize the state. For the exact ground state, the above formula simplifies to

$$g_n = \frac{2}{L} \sum_{k=0}^{(L-1)/2} \frac{h\cos n\theta_k + J\cos(n+1)\theta_k}{E_k} \tag{10}$$

$$\tag{11}$$

The entanglement entropy of a region A can be obtained by restricting the correlation matrix Γ to a region A of size L_A. The eigenvalues of the reduced Γ_A, denoted with ν_m, contribute equally to the entanglement entropy through

$$\begin{aligned} S(L_A) = &- \sum_\nu \left(\frac{1+\nu_m}{2}\right) \log_2 \left(\frac{1+\nu_m}{2}\right) \\ &+ \sum_\nu \left(\frac{1-\nu_m}{2}\right) \log_2 \left(\frac{1-\nu_m}{2}\right) \end{aligned}$$

This method scales polynomially in the system size L, allowing the study of systems with hundreds of spins.

Figure 1 shows the EE of our ansatz converges to the Cardy formula [4] as P increases .

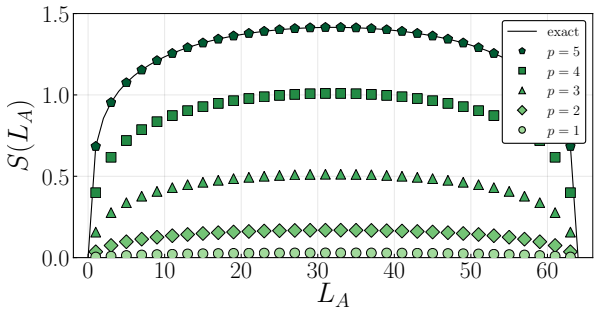

FIG. 1. Entanglement entropy as a function of subsystem size L_A for intermediate p states in a depth $P = 5$ ansatz for $L = 64$ spins.

The spin-spin correlation functions can also be computed from g_n.

$$\langle X_0 X_n \rangle = g_0^2 - g_n g_{-n}$$

$$\langle Z_0 Z_n \rangle = \det \begin{pmatrix} g_{-1} & g_{-2} & \cdots & g_{-n} \\ g_0 & g_{-1} & \cdots & g_{1-n} \\ \vdots & \vdots & \ddots & \vdots \\ g_{n-2} & g_{n-3} & \cdots & g_{-1} \end{pmatrix}$$

Figure 2 shows the spin-spin correlations for $P = 5$ at the critical point $h/J = 1$.

ABSENCE OF LIGHT-CONE IN IMAGINARY TIME EVOLUTION

Here we provide an analytical demonstration that the light cone is not observed in the imaginary time evolution of a pure state. Consider the set-up of a local quench in a $(1+1)$-dimensional CFT described in Ref. [5]. For $t < 0$, the system consists of two semi-infinite disjoint regions with identical Hamiltonians which are in their respective ground states. At $t = 0$, the two regions are joined at a point which we choose as the origin. We are interested in the time-evolution of the entanglement entropy for the subregion $-\infty < x < -\ell$ with the rest of the subsystem (i.e., $-\ell < x < \infty$). As shown in Ref. [5], for real time evolution, the entanglement entropy takes the following form:

$$S = \begin{cases} \frac{c}{6} \log\left(2\ell/a\right) + c_1 & t < \ell \\ \frac{c}{6} \log\left(\frac{t^2-\ell^2}{a^2}\right) + c_2 & t > \ell \end{cases} \tag{12}$$

where a is the short-distance cut-off and c_1, c_2 are constants. The qualitative difference between $t < \ell$ and $t > \ell$ originates precisely due to the locality of interactions, which results in a sharp light-cone in the continuum field theory, and a Lieb-Robinson light cone on a lattice-regularized CFT. Heuristically, for $t < \ell$, the quasi-particles generated at location $x = -\ell$ haven't had enough time to reach the entangling boundary.

Next we consider the same set-up except that one evolves the system with imaginary time, which we denote as τ. Mathematically, if we denote the Hamiltonians for $x < 0$ and $x > 0$ as H_1, H_2, and the Hamiltonian that connects the two regions at the origin as H_{12}, the unnormalized wavefunction for $\tau > 0$ is given by $|\psi(\tau)\rangle = e^{-\tau(H_1+H_2+H_{12})}|\psi(0)\rangle$ where $|\psi(0)\rangle$ is the ground state of $H_1 + H_2$. One can obtain the time-dependence of entanglement entropy following the technique identical to Ref. [5]. One finds:

$$S = \frac{c}{6} \log\left(\frac{2\sqrt{\ell^2+\tau^2}}{a}\right) + c_1 \tag{13}$$

Therefore, although both the real time and the imaginary time entanglement grows logarithmically for times much larger than ℓ, there is no signature of light-cone in the imaginary time growth of entanglement, and the entanglement entropy starts to increase instantaneously following the quench.

For completeness, we also discuss imaginary time entanglement growth under a global quench. We now consider the set-up of Ref. [4], where the initial state $|\psi_0\rangle$ is taken to be short-ranged entangled and corresponds to a translationally invariant conformal boundary condition. It was shown in Ref. [4] that for *real* time evolution of the state $|\psi_0\rangle$ with the CFT Hamiltonian, the entanglement of a region of size ℓ grows as:

$$S \sim \begin{cases} \frac{\pi c t}{6a}, & t < \ell/2 \\ \frac{\pi c \ell}{12a}, & t > \ell/2 \end{cases} \tag{14}$$

Therefore, the entanglement becomes volume-law after time $t = \ell/2$, which can again be understood from a quasi-particle picture. However, under imaginary time evolution, using technique identical to Ref. [4] one instead finds:

$$S \sim \frac{c}{6}\left[\log\left(\frac{2\tau}{\pi}\right) + \log\left(\frac{e^{\pi\ell/4\tau} - e^{-\pi\ell/4\tau}}{e^{\pi\ell/4\tau} + e^{-\pi\ell/4\tau}}\right)\right] \tag{15}$$

Therefore, for $\tau \ll \ell$, $S \sim \frac{c}{3}\log(\tau)$ while, as expected, for $\tau \gg \ell$, $S \sim \frac{c}{3}\log(\ell)$, the ground state entanglement corresponding to the CFT.

QUANTUM TO CLASSICAL MAP

The foundation of path integral world-line Monte Carlo is the connection between a quantum system in

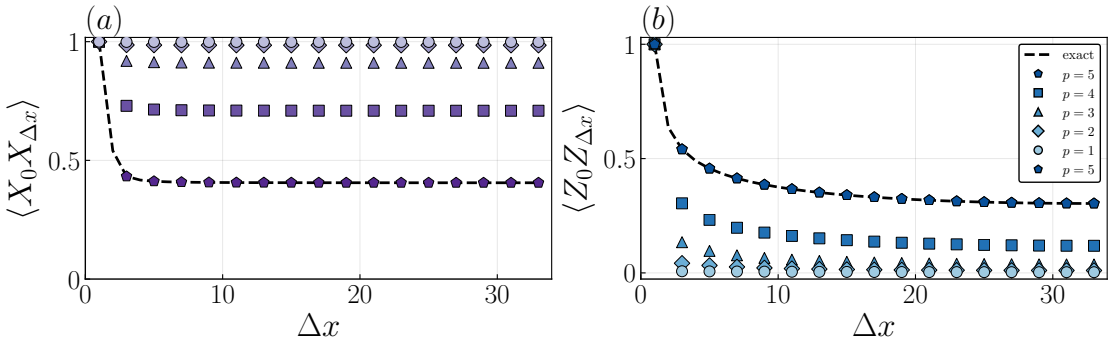

FIG. 2. Spin-spin correlation functions for intermediate p states in a depth $P = 5$ ansatz for $L = 64$ spins.

d-dimensions and a classical statistical one in $(d + 1)$-dimensions. In our case, we wish to consider the variational quantum state given by

$$|\psi_P(\boldsymbol{\alpha},\boldsymbol{\beta})\rangle = \mathcal{N}\prod_{p=P}^{1} e^{-\beta_p H_X} e^{-\alpha_p H_{ZZ}} |+\rangle \tag{16}$$

where we include the H_Z term for generality.

In the following, we will only consider $P = 1$, but the higher-P formulation is nearly identical. The expectation value of some operator $\mathcal{O}$, up to a normalization, is

$$\begin{aligned}\langle\mathcal{O}\rangle &= \langle\psi_P(\boldsymbol{\alpha},\boldsymbol{\beta})|\,\mathcal{O}\,|\psi_P(\boldsymbol{\alpha},\boldsymbol{\beta})\rangle \\ &= \langle+|e^{-\alpha_1 H_{ZZ}} e^{-\beta_1 H_X}\mathcal{O} e^{-\beta_1 H_X} e^{-\alpha_1 H_{ZZ}}|+\rangle \\ &= \sum_{\{s\}}\sum_{i=1}^{L}\sum_{p=1}^{2P+1}\tilde{\mathcal{O}}(s_{i,p})\,p(s_{i,p})\end{aligned} \tag{17}$$

The probability $p(s_{i,p})$ is the Boltzmann factor, given by the exponential of the Hamiltonian

$$H_{\rm 2D} = -\sum_{i=1}^{L}\sum_{p=1}^{2P+1}\left(J_x(p)s_{i,p}s_{i+1,p} + J_t(p)s_{i,p}s_{i,p+1}\right) \tag{18}$$

up to a normalization $Z = \sum e^{-H_{\rm 2D}}$, where the couplings of the classical model are related to $(\boldsymbol{\alpha},\boldsymbol{\beta})$ via

$$J_x(p) = \alpha_p \tag{19}$$

$$J_t(p) = \frac{1}{2}\ln\coth\beta_p \tag{20}$$

Continuing this process for higher P is straightforward, and can be visualized as a $L \times (2P + 1)$ lattice in Fig. 3. Adding connections $J_x(0)$ between the middles time-slices ($p = P + 1$) one obtains the Suzuki-Trotter inspired neural networks in Ref. [6].

The only observables required to compute the total energy are:

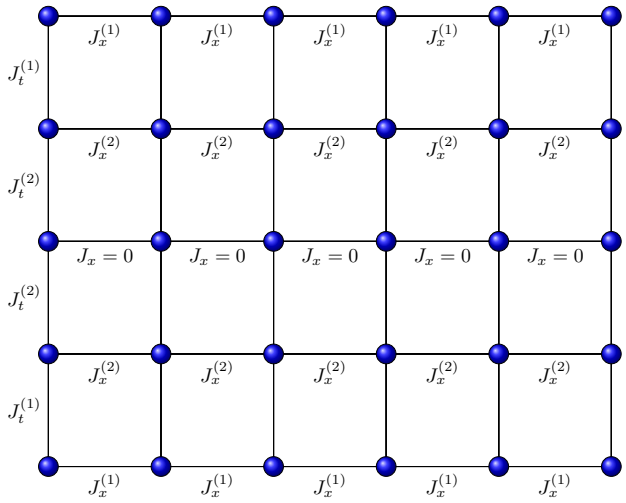

FIG. 3. Schematic of the two-dimensional classical Ising lattice dual to the ansatz in Eq. (16) for depth $P = 2$ and $L = 6$ spins.

$$\langle Z_i Z_{i+1}\rangle = \sum_{\{\mathbf{s}\}} s_{i,m}\, s_{i,m}\, p(s_{i,p}) \tag{21}$$

$$\langle X_i\rangle = \sum_{\{\mathbf{s}\}} \exp(-2J_t(m)\, s_{i,m}, s_{i,m}) p(s_{i,p}) \tag{22}$$

where $m = P + 1$ denotes the middle time-slice.

The gradients of these expressions can be evaluated via

$$\partial_\theta\langle H\rangle = \langle\partial_\theta H\rangle - \langle H\partial_\theta E(\boldsymbol{\theta})\rangle + \langle E(\boldsymbol{\theta})\rangle\langle H\rangle \tag{23}$$

where $E(\boldsymbol{\theta})$ is the energy of the classical Ising model, and $\boldsymbol{\theta}$ denotes $(\boldsymbol{\alpha},\boldsymbol{\beta})$. The exponential form of Eq. (16) make stochastic reconfiguration (SR) [7], easy to implement. SR uses the positive-definite covariance matrix S as a pre-conditioner for the gradient where S is defined as

$$S_{\theta,\theta'} = \langle\mathcal{O}_\theta\mathcal{O}_{\theta'}\rangle - \langle\mathcal{O}_\theta\rangle\langle\mathcal{O}_{\theta'}\rangle\ ,$$

with $\mathcal{O}_\theta = \partial_\theta(\log\psi(\boldsymbol{\theta}))$.

Each gradient update then takes the form

$$\theta \leftarrow \theta - \eta S^{-1} \partial_\theta \langle H \rangle \tag{24}$$

for a small learning rate η which we take to decay during iteration. It is possible that S is non-invertible so we use the Moore-Penrose pseudo-inverse.

We typically find optimizing $P = 1$ converges rapidly, while higher-P becomes more difficult. Optimal parameters for a fixed P vary smoothly with system size and field strength, which makes inferring 'nearly' optimal parameters easy (Fig. 4). This result is highly similar to the patterns in optimal parameters found in Ref. [8] for QAOA.

IMAGINARY TIME REQUIRED TO PREPARE GHZ STATE FROM PARAMAGNET

Consider the case of preparing the GHZ state $|\mathrm{GHZ}\rangle$, from the paramagnet $|+\rangle$ using the projection in imaginary time, $e^{-\tau H_{ZZ}}$. We will show that the total time τ required scales with $\log L$.

Suppose that after time τ, the infidelity between the target and projected state is ϵ,

$$|\langle \mathrm{GHZ}|e^{-\tau H_{ZZ}}|+\rangle|^2 = 1 - \epsilon\,. \tag{25}$$

Setting the energy of all up spins (or all down) to zero, the squared norm of the projected state, $e^{-\tau H_{ZZ}}|+\rangle$, is the partition function of the 1d Ising model at inverse temperature 2τ:

$$\mathcal{Z} = (1 - 1/x)^L + (1 + 1/x)^L\,,$$

where $x \equiv e^{4\tau}$.

Taking the limit $L \to \infty$ with $x = \alpha L$, we find that $\mathcal{Z} = 2\cosh(1/\alpha)$. Therefore we satisfy Eq. (25) if $\alpha^{-1} = \cosh^{-1}((1-\epsilon)^{-1})$, and $\tau = \log(\alpha L)/4$.

ERROR IN FIDELITY PROVIDES A BOUND ON ERROR IN OBSERVABLES

Let ψ_t denote the target state and consider a wavefunction ψ such that $1 - |\langle \psi_t|\psi\rangle|^2 < \epsilon$. Then there exists $\psi_t^\perp$ such that $\psi = \sqrt{1-\epsilon}\psi_t + \sqrt{\epsilon}\psi_t^\perp$. Hence, for any observable O,

$$\begin{aligned}\langle\psi|O|\psi\rangle =& (1-\epsilon)\langle\psi_t|O|\psi_t\rangle \\ &+2\sqrt{\epsilon(1-\epsilon)}Re\big(\langle\psi_t^\perp|O|\psi_t\rangle\big) + \epsilon\langle\psi_t^\perp|O|\psi_t^\perp\rangle\end{aligned}$$

If the operator norm of O is $c \equiv \sup_{|v\rangle\neq 0}\frac{||O|v\rangle||}{|||v\rangle||}$, then

$$|\langle\psi|O|\psi\rangle - \langle\psi_t|O|\psi_t\rangle| \le 2c\left(\sqrt{\epsilon(1-\epsilon)} + \epsilon\right).$$

[1] Elliott Lieb, Theodore Schultz, and Daniel Mattis, "Two soluble models of an antiferromagnetic chain," Annals of Physics **16**, 407–466 (1961).

[2] Ingo Peschel, "Calculation of reduced density matrices from correlation functions," Journal of Physics A: Mathematical and General **36**, L205–L208 (2003).

[3] G. Vidal, J. I. Latorre, E. Rico, and A. Kitaev, "Entanglement in quantum critical phenomena," Physical Review Letters **90** (2003), 10/chw37f; J. I. Latorre, E. Rico, and G. Vidal, "Ground State Entanglement in Quantum Spin Chains," Quantum Info. Comput. **4**, 48–92 (2004).

[4] Pasquale Calabrese and John Cardy, "Evolution of entanglement entropy in one-dimensional systems," Journal of Statistical Mechanics: Theory and Experiment **2005**, P04010 (2005).

[5] Pasquale Calabrese and John Cardy, "Entanglement and correlation functions following a local quench: A conformal field theory approach," Journal of Statistical Mechanics: Theory and Experiment **2007**, P10004–P10004 (2007).

[6] Nahuel Freitas, Giovanna Morigi, and Vedran Dunjko, "Neural network operations and Susuki–Trotter evolution of neural network states," International Journal of Quantum Information **16**, 1840008 (2018).

[7] Federico Becca and Sandro Sorella, *Quantum Monte Carlo Approaches for Correlated Systems*, 1st ed. (Cambridge University Press, Cambridge, United Kingdom ; New York, NY, 2017).

[8] Leo Zhou, Sheng-Tao Wang, Soonwon Choi, Hannes Pichler, and Mikhail D. Lukin, "Quantum Approximate Optimization Algorithm: Performance, Mechanism, and Implementation on Near-Term Devices," arXiv:1812.01041 [cond-mat, physics:quant-ph] (2018).

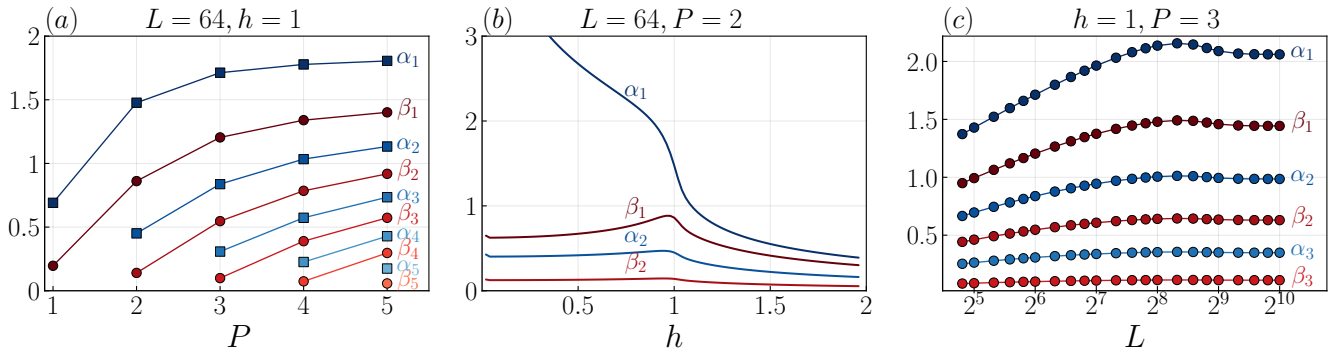

FIG. 4. Optimal parameters $(\boldsymbol{\alpha}, \boldsymbol{\beta})$ found using the Jordan-Wigner method for $L = 64$ spins for (a) the critical point $h = 1$ with $P = 1, ..., 5$, (b) Optimal parameters for $P = 2$ for various h, (c) scaling of optimal parameters with L at $h = 1$. All plots are generic for any P and system size L.